Effect of Anisotropic Hybridization in $YbAlB_4$ Probed by Linear Dichroism in Core-Level Hard X-Ray Photoemission Spectroscopy

Kentaro Kuga,[1] Yuina Kanai,[1,2] Hidenori Fujiwara,[1,2] Kohei Yamagami,[1,2] Satoru Hamamoto,[1,2] Yuichi Aoyama,[1,2] Akira Sekiyama,[1,2] Atsushi Higashiya,[1,3] Toshiharu Kadono,[1,4] Shin Imada,[1,4] Atsushi Yamasaki,[1,5] Arata Tanaka,[6] Kenji Tamasaku,[1] Makina Yabashi,[1] Tetsuya Ishikawa,[1] Satoru Nakatsuji,[7,8] and Takayuki Kiss[1,2]

[1]*RIKEN SPring-8 Center, Sayo, Hyogo 679-5148, Japan*
[2]*Graduate School of Engineering Science, Osaka University, Toyonaka, Osaka 560-8531, Japan*
[3]*Faculty of Science and Engineering, Setsunan University, Neyagawa, Osaka 572-8508, Japan*
[4]*College of Science and Engineering, Ritsumeikan University, Kusatsu, Shiga 525-8577, Japan*
[5]*Faculty of Science and Engineering, Konan University, Kobe, Hyogo 658-8501, Japan*
[6]*Department of Quantum Matter, ADSM, Hiroshima University, Higashi-Hiroshima, Hiroshima 739-8530, Japan*
[7]*The Institute for Solid State Physics, The University of Tokyo, Kashiwa, Chiba 277-8581, Japan*
[8]*CREST, Japan Science and Technology Agency (JST), 4-1-8 Honcho Kawaguchi, Saitama 332-0012, Japan*

(Received 19 November 2018; published 17 July 2019)

We have probed the crystalline electric-field ground states of pure $|J = 7/2, J_z = \pm 5/2\rangle$ as well as the anisotropic c-f hybridization in both valence fluctuating systems α- and β-$YbAlB_4$ by linear polarization dependence of angle-resolved core level photoemission spectroscopy. Interestingly, the small but distinct difference between α- and β-$YbAlB_4$ was found in the polar angle dependence of linear dichroism, indicating the difference in the anisotropy of c-f hybridization, which may be a key to understanding a heavy Fermi liquid state in α-$YbAlB_4$ and a quantum critical state in β-$YbAlB_4$.

DOI: 10.1103/PhysRevLett.123.036404

The crystalline electric field (CEF) ground state (GS) regulates physical properties at low temperatures and sometimes leads to a variety of nontrivial quantum states such as quantum criticality in the quadrupolar Kondo lattice system [1–3], colossal magnetoresistance, and high temperature superconductivity in transition metal oxides [4]. For example, in a high T_c cuprate, CEF splitting of a Cu $3d$ electron determines the half filling in the $d_{x^2-y^2}$ orbital, which anisotropically hybridizes with neighboring O $2p$ electrons, mediating electric and magnetic interaction [5]. Such an anisotropic hybridization of the orbital selected by CEF plays an essential role in the physical properties in many of the transition metal oxides [4]. An accurate estimation of CEF GS and hybridization is indispensable to understand the underlying mechanisms.

In rare-earth metal systems, it is essential to determine the CEF GS yielding rich variety of the unconventional low temperature properties. One of the most interesting phenomena is a quantum criticality in β-$YbAlB_4$ which stems from the "pure" $|J = 7/2, J_z = \pm 5/2\rangle$ CEF GS and the nodal hybridization in momentum space as predicted by Ramires *et al.* [6]. In this theory, a new type of topological phase transition in the Fermi surface is predicted to arise and induces a topological nontrivial vortex metal that shows magnetic properties of $T^{-1/2}$ divergence and T/B scaling.

β-$YbAlB_4$ is a fascinating and mysterious material that is the first discovered superconductor in the Yb-based heavy fermion systems [7,8], and shows quantum criticality without tuning [9] in the strongly valence fluctuating state [10]. Furthermore, the quantum criticality at ambient pressure survives up to 0.4 GPa, forming a non-Fermi-liquid phase [11]. To understand the underlying mechanism, laser ARPES probed anisotropic hybridization as a momentum dependent Kondo hybridization band that is consistent with the nodal hybridization model [12]. CEF GS is also reported to be consistent with the $|\pm 5/2\rangle$ state estimated by the temperature dependence of magnetic susceptibility [13]. Indeed, the $|\pm 5/2\rangle$ state is plausible because the distribution of the $4f$ hole extends toward neighboring heptagonal rings of boron atoms, maximizing the hybridization with boron rings. However, the analysis of the temperature dependence of magnetic susceptibility is not straightforward because β-$YbAlB_4$ has a strong valence fluctuation due to the strong c-f hybridization [10]. The low symmetric orthorhombic crystal structure in β-$YbAlB_4$ also makes it quite difficult to analyze CEF accurately because of many of the CEF parameters. Thus, no definitive experimental results including the estimation of the admixture with other J_z components are reported.

Recently the CEF GSs of several lanthanide based materials have been probed by the angle-resolved core-level hard x-ray photoemission spectroscopy (HAXPES) using linearly polarized light. Linear dichroism (LD), which is defined as the spectral difference of the photoemission spectra obtained by the s- and p-polarized configuration as shown in Fig. 1(b), reflects the anisotropic charge

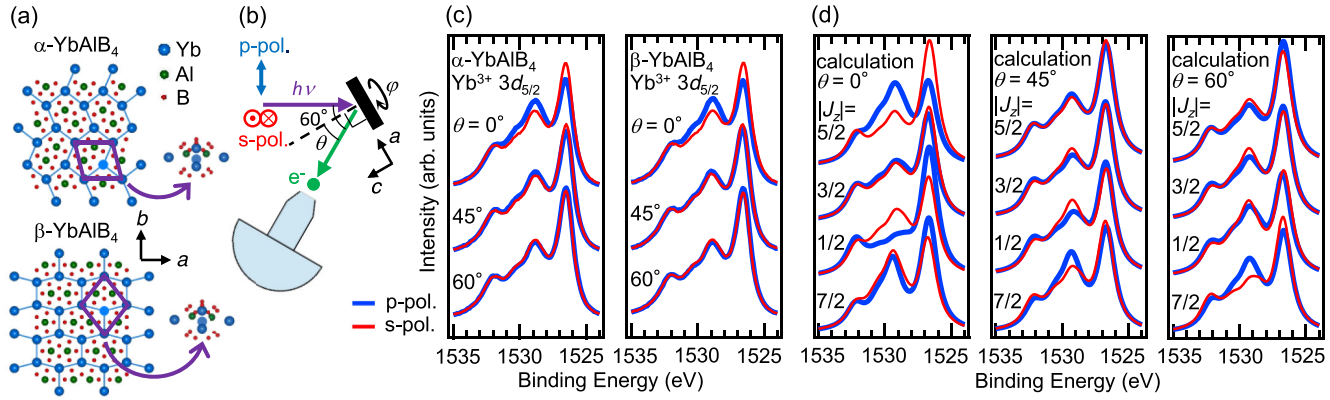

FIG. 1. (a) Crystal structure of α- and β-$YbAlB_4$ with a view along the c axis. The Yb-Al layer is sandwiched by heptagonal and pentagonal B layers, respectively. The local structures surrounded by the purple quadrangles are shown at the right side as the pictorial views that are oriented to the acute angles of the quadrangles. (b) Schematic top view geometry of incident horizontally (blue arrow) and vertically (red arrow) polarized x rays, sample, and photoelectron analyzer. Polar angle θ is defined as an angle between the directions toward the photoelectron analyzer and the c axis of the sample, and $\theta = 60°$ corresponds that the c axis is oriented toward the incident x ray. Azimuthal angle φ is defined as the angle of the rotation along the c axis and $\varphi = 0°$ corresponds to the geometry as drawn in Fig. 1(b). (c) Polarization-dependent Yb^{3+} $3d_{5/2}$ core-level HAXPES spectra of α- and β-$YbAlB_4$ with the polar angle of $\theta = 0°$, 45°, and 60°. Red thin and blue thick lines correspond to s and p polarization. The spectra are normalized by the spectral weight of Yb^{3+} $3d_{5/2}$ after the subtraction of Shirley-type backgrounds [18,19]. (d) Ionic calculation of polarization-dependent Yb $3d_{5/2}$ core-level HAXPES spectra of pure J_z states of a $4f$ hole at each θ.

distribution of the $4f$ hole through the interaction with the core hole created in the optical process [14]. For example, in Yb based materials, LDs of Yb $3d$ core-level multiplet structures determined the GSs of the cubic system YbB_{12} as Γ_8 and the GSs of the tetragonal systems $YbRh_2Si_2$ and $YbCu_2Si_2$ as $|\pm 3/2\rangle$ and $-0.36|\pm 5/2\rangle + 0.93|\mp 3/2\rangle$, respectively [15,16]. This method is also applicable to the lower symmetric systems. In this Letter, we show the experimental evidence of pure $|\pm 5/2\rangle$ CEF GS of the orthorhombic β-$YbAlB_4$ probed by the polar angle and azimuthal angle dependence of LDs of Yb $3d$ HAXPES spectra. In addition, we found the importance of explicit anisotropic hybridization between $4f$ and conduction electrons to describe the CEF of β-$YbAlB_4$. For comparison, we also measured the stoichiometric compound α-$YbAlB_4$, which shows a heavy Fermi liquid ground state [17].

In α- and β-$YbAlB_4$, local symmetry at the Yb site is C_s and C_{2v}, respectively [20]. However, the regions surrounded by the four neighboring Yb sites resemble in both systems as shown in the purple quadrangles and their pictorial views in Fig. 1(a). Therefore, we can approximate that the local symmetry at the Yb site in α-$YbAlB_4$ is C_{2v} and a similar CEF GS is expected, which turned out to be true. The $J = 7/2$ states of Yb^{3+} $4f$ electron in C_{2v} symmetry will split into four doublets and C_{2v} CEF is expressed by B_2^0, B_2^2, B_4^0, B_4^2, B_4^4, B_6^0, B_6^2, B_6^4, and B_6^6 in Stevens' formalism [21]. These parameters will produce the eight eigenfunctions expressed by using J_z as $a_i|\pm 5/2\rangle + b_i|\mp 3/2\rangle + c_i|\pm 1/2\rangle + d_i|\mp 7/2\rangle (i = 1 \sim 4)$, where $a_i^2 + b_i^2 + c_i^2 + d_i^2 = 1$. For the simple comparison between measurement and calculation, we have performed an ionic calculation including the full multiplet theory and the local CEF splitting using the XTLS 9.0 program [22,23]. Atomic parameters such as the $4f$-$4f$ and $3d$-$4f$ Coulomb and exchange interactions (Slater integrals) and the spin-orbit couplings were obtained using Cowan's code based on the Hartree-Fock method [24]. The Slater integrals and spin-orbit couplings are reduced to 88% and 98% according to Refs. [15,16,25]. The single impurity Anderson model (SIAM) was also employed for the calculation which includes explicit c-f hybridization [26,27].

We performed polarization-dependent Yb $3d$ core-level HAXPES with a MBS A1-HE hemispherical photoelectron spectrometer at BL19LXU of SPring-8 [28,29]. Horizontally polarized x-ray radiation produced by a 27-m-long undulator was monochromated to be 7.9 keV by a Si (111) double crystal and a Si(620) channel-cut crystal. To switch the excitation light from horizontal to vertical polarization for LD, we used two diamond(100) single crystals as a phase retarder and vertically polarized component of the x ray was 98% [30]. Since the direction of the photoelectron analyzer was in the horizontal plane with an angle about an incident x ray of 60° as shown in Fig. 1(b), vertically polarized and horizontally polarized x rays correspond to s- and p-polarization geometry, respectively. The details of sample preparation and characterization are described in the Supplemental Material [31]. The experimental geometry was controlled by using a two-axis manipulator which equips polar and azimuthal rotations [30]. The energy resolution was set to ~400 meV. The sample temperature was set to 25 K, which is sufficiently lower than the first excited energy confirmed by negligible

temperature dependence up to 60 K for β-$YbAlB_4$ (see Supplemental Material for details [31]).

Figure 1(c) is the polarization-dependent Yb^{3+} $3d_{5/2}$ core-level HAXPES spectra of α- and β-$YbAlB_4$ with polar angle of $\theta = 0°$, 45°, and 60° as drawn in Fig. 1(b). The multiplet structures peak at 1526, 1529, and 1532 eV with polarization and θ dependences that reflect the charge distribution of $4f$ holes. The polarization and θ dependences in α- and β-$YbAlB_4$ are similar, suggesting almost the same CEF GS as expected from the local arrangement of neighboring atoms [Fig. 1(a)]. Peaks at 1526 eV with s-polarization geometry (s-pol.) are higher than those of the p-polarization geometry (p-pol.) at $\theta = 0°$. This difference becomes smaller at 45° and the sign changes at 60°. For the peaks at 1529 eV, these magnitude relations are reversed. According to the ionic calculation shown in Fig. 1(d), all the magnitude relations in addition to the comparably large LD at $\theta = 0°$ are consistent with only the $|\pm 5/2\rangle$ state. However, the magnitude of the LDs are about 3 times smaller than those of the ionic calculation at $\theta = 0°$ and 60°. These comparisons suggest that the main component of the wave functions in α- and β-$YbAlB_4$ is $|\pm 5/2\rangle$. The possible reasons for the quantitative differences are the admixture with other J_z components and/or c-f hybridization because both effects will deform the charge distribution of the $4f$ hole and will change LD. The other extrinsic reasons such as the backscattering effect of the photoelectrons [32] are discussed in the Supplemental Material and all of their effects turned out to be negligibly small [31].

First, we focus on the mixing effect, namely, $|\pm 5/2\rangle$ plus $|\mp 3/2\rangle$, $|\pm 1/2\rangle$, and/or $|\mp 7/2\rangle$. The pure $|\pm 5/2\rangle$ state shows no rotational dependence in LDs along the c axis as shown in Fig. 2(c) because of the isotropic charge distribution around the c axis. On the other hand, mixed states induce the azimuthal angle dependence as shown in $CeCu_2Ge_2$ [37], except the binary mixed state with $|\mp 7/2\rangle$. However, it is unnatural if the wave function is $|\pm 5/2\rangle$ plus $|\mp 7/2\rangle$ because the CEF Hamiltonian must have tetragonal symmetric terms of the pure $|\pm 5/2\rangle$ state plus the sixfold symmetric term B_6^6 and other orthorhombic terms B_2^2, B_4^2, and B_6^2 must be zero. Therefore we can distinguish if the CEF GS is the pure $|\pm 5/2\rangle$ state or the mixed state by measuring the azimuthal angle dependence of LDs.

Figures 2(a)–2(c) show the Yb^{3+} $3d_{5/2}$ core-level HAXPES spectra with different azimuthal angles φ and with the fixed polar angle of $\theta = 60°$ in α-$YbAlB_4$, β-$YbAlB_4$, and their LDs, respectively. For both α- and β-$YbAlB_4$, the azimuthal angle dependences of LD are negligible within the experimental noise, indicating the pure $|\pm 5/2\rangle$ state. The error bars of the wave function can be estimated by ionic calculation for the binary mixed states as shown in Fig. 2(c). In the case of the $|\pm 5/2\rangle$ plus (minus) $|\mp 3/2\rangle$ state, fourfold symmetric azimuthal angle

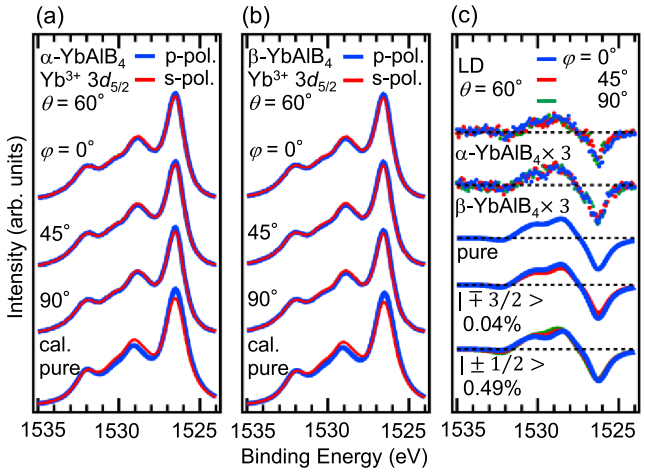

FIG. 2. (a) and (b) The azimuthal angle dependence of Yb^{3+} $3d_{5/2}$ core-level HAXPES spectra in α- and β-$YbAlB_4$ at $\theta = 60°$ and the ionic calculation of the pure $|\pm 5/2\rangle$ state. (c) The azimuthal angle dependence of LDs in α- and β-$YbAlB_4$ (closed circle) and the ionic calculation for pure $|\pm 5/2\rangle$ state and $|\pm 5/2\rangle$ plus a small amount of $|\mp 3/2\rangle$ ($\sim 0.9998|\pm 5/2\rangle + 0.02|\mp 3/2\rangle$) or $|\pm 1/2\rangle$ ($\sim 0.9975|\pm 5/2\rangle + 0.07|\pm 1/2\rangle$) state (solid line). LD is defined as the difference of normalized intensity between the s and p polarization. The amplitude of LDs of α- and β-$YbAlB_4$ is multiplied by three to compare with the calculations.

dependence appears and LDs at $\varphi = 0°$ and 90° overlap and LD at $\varphi = 45°$ is smaller (larger) than others. The azimuthal angle dependence is very sensitive and the experimental statistics suggests that the maximum possible component of $|\mp 3/2\rangle$ is only 0.04%, indicating that LD by HAXPES is an extremely sensitive probe of the electronic state. On the other hand, the $|\pm 5/2\rangle$ plus (minus) $|\pm 1/2\rangle$ state must show twofold symmetry in the azimuthal angle dependence of LDs, and LD at 1529 eV increases (decreases) as φ changes from 0° to 90°. Since the azimuthal angle dependence is less sensitive within the experimental statistics, the maximum possible component of $|\pm 1/2\rangle$ is estimated as 0.49%. If $|\mp 3/2\rangle$ and/or $|\pm 1/2\rangle$ are mixed in addition to $|\mp 7/2\rangle$, $|\mp 7/2\rangle$ can have a finite contribution because the orthorhombic CEF parameters of B_2^2, B_4^2, and B_6^2 do not have to be all zero in contrast to the binary mixed state with $|\mp 7/2\rangle$ as we explained above. However, the contribution would be much smaller than that of the $|\mp 3/2\rangle$ and/or $|\pm 1/2\rangle$ states, resulting in the error bar much less than that of $|\mp 3/2\rangle$ or $|\mp 1/2\rangle$. As these tiny error bars cannot explain the huge difference of LDs between the experiment and calculation by the ionic model, we can conclude that the LDs in α- and β-$YbAlB_4$ are modified by c-f hybridization. Note that the c-f hybridization must be φ independent because the anisotropy in c-f hybridization will yield anisotropic LDs.

As α- and β-$YbAlB_4$ are strongly valence fluctuating systems with the Yb valences of 2.73 and 2.75 [10], strong c-f hybridization is expected to modify LD, which was not apparently observed in YbB_{12}, $YbRh_2Si_2$, and $YbCu_2Si_2$

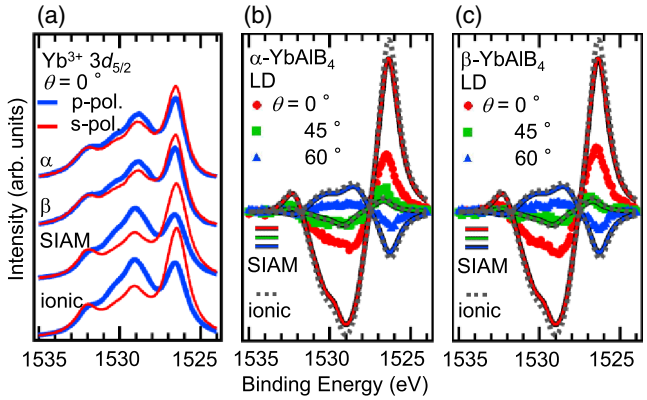

FIG. 3. (a) Polarization-dependent Yb^{3+} $3d_{5/2}$ core-level HAXPES spectra of α- and β-$YbAlB_4$ at $\theta = \varphi = 0°$, and the calculation of the spectra for $|\pm 5/2\rangle$ state based on SIAM including isotropic c-f hybridization. (b) and (c) The experimental LDs (closed circle, square, and triangle) of α- and β-$YbAlB_4$ and the calculation for $|\pm 5/2\rangle$ state based on the SIAM (solid line) and ionic model (broken line). Red, green, and blue lines on the black lines correspond to the LDs by SIAM at $\theta = 0°$, 45°, and 60°. The same parameters are used in the calculations shown in (b) and (c).

[15,16]. To take into account the mixed valence state between Yb^{3+} ($4f^{13}$) and Yb^{2+} ($4f^{14}\underline{L}$), where $\underline{L}$ denotes the conduction band with one hole, the calculation based on SIAM for the $|\pm 5/2\rangle$ state has been employed with isotropic c-f hybridization. Figure 3(a) shows the Yb^{3+} $3d_{5/2}$ core-level HAXPES spectra of α-$YbAlB_4$, β-$YbAlB_4$, and calculation by SIAM and the ionic model at $\theta = \varphi = 0°$. The parameters of the Coulomb interaction between the $4f$ electrons and $3d$ core hole U_{fc} and the effective $4f$ binding energy Δ_f and isotropic c-f hybridization strength V_{eff} were set to be 10.0, 0.5, and 1.0 eV. The peaks of the multiplet by SIAM is slightly wider than those of the ionic model and the multiplet structure will drastically change if the V_{eff} is larger than 2.0 eV (not shown). Figure 3(b) and 3(c) show experimental LDs of α- and β-$YbAlB_4$ and the calculated LDs by SIAM and ionic model. For all geometry, calculations by SIAM show 1.15 times smaller LDs than that of ionic model. The ratio of the integrated intensity of LDs from 1528 to 1534 eV between experiments of α-$YbAlB_4$ (β-$YbAlB_4$) and calculations by SIAM with isotropic hybridization are 2.9 (2.6), 0.68 (1.0), and 3.6 (3.2) for $\theta = 0°$, 45° and 60°, respectively. These comparisons indicate the importance of anisotropic c-f hybridization to understand the CEF in α- and β-$YbAlB_4$, which easily deforms the charge distribution as well as the LDs like oxides. Furthermore, we can see the larger anisotropy in LDs of α-$YbAlB_4$, indicating the different anisotropy in c-f hybridization that is integrated into CEF.

Our experiments with α- and β-$YbAlB_4$ have probed the CEF GSs of pure $|\pm 5/2\rangle$ with the polar angle θ dependent and azimuthal angle φ independent c-f hybridizations. These results remind us of the topological nontrivial vortex metallic state originating from nodal hybridization in momentum space, which is predicted in β-$YbAlB_4$ [6]. Experimental support of this nodal hybridization has been reported where laser ARPES measurement for β-$YbAlB_4$ probed two anticrossings of $4f$ CEF levels with dispersive conduction band in which momentum dependence is consistent with the nodal hybridization model [12]. On the other hand, for α-$YbAlB_4$, no clear Kondo hybridization band like β-$YbAlB_4$ was observed by laser ARPES. In our measurement of LD for α-$YbAlB_4$, we observed clear c-f hybridization in the Yb $4f$ $|\pm 5/2\rangle$ state possibly because Yb $3d_{5/2}$ core-level HAXPES reflects a local feature compared with the valence band measured by ARPES. Furthermore, we discovered that the LD at each θ in β-$YbAlB_4$ has a slightly smaller deviation from calculation than the LD in α-$YbAlB_4$ as shown in Figs. 3(b) and 3(c), indicating that β-$YbAlB_4$ has the slightly smaller anisotropy of c-f hybridization. Our establishment of the similarity in the CEF GSs of pure $|\pm 5/2\rangle$ with very small error bars of less than 0.5% and the subtle difference in anisotropic c-f hybridization will help finding the key point to understand the mechanism of the quantum critical state in β-$YbAlB_4$ and the Fermi liquid state in α-$YbAlB_4$. Furthermore, our solution of an accurate probe for CEF GS in a strongly valence fluctuating and a Yb-based low symmetric system is attractive to other strongly correlated electron systems such as α-$YbAl_{1-x}Fe_xB_4$ and the Yb-Al-Au approximant crystal and quasicrystal [38,39]. As we have shown the existence of anisotropy in c-f hybridization, the detailed angle-resolved core level LDs by HAXPES can be a new probe of anisotropic c-f hybridization in real space.

We thank S. Fujioka, H. Aratani, T. Hattori, H. Yomosa, S. Takano, T. Kashiuchi, K. Nakagawa, K. Sakamoto, and Y. Kobayashi for support in experiments. We also thank H. Kobayashi for useful discussions. Sample preparation was carried out under the Visiting Researcher's Program of the Institute for Solid State Physics, the University of Tokyo. HAXPES experiments were performed at BL19LXU in SPring-8 with the approval of RIKEN (Proposals No. 20160034, No. 20160066, No. 20170043, No. 20170081, No. 20180026, and No. 20180076). This work is supported by a Grant-in-Aid for Scientific Research (16H04014, 16H04015, 18K03512), and a Grant-in-Aid for Innovative Areas (16H01074, 18H04317) from MEXT and JSPS, Japan. This work is partially supported by CREST (JPMJCR15Q5, JPMJCR18T3), Japan Science and Technology Agency, by Grants-in-Aid for Scientific Research (16H02209), and by Grants-in-Aids for Scientific Research on Innovative Areas (15H05882, 15H05883) from MEXT. Y. K. was supported by the JSPS Research Fellowships for Young Scientists.

[1] D. L. Cox, Phys. Rev. Lett. **59**, 1240 (1987).
[2] D. L. Cox and M. Makivic, Physica (Amsterdam) **199B–200B**, 391 (1994).
[3] H. Kusunose, K. Miyake, Y. Shimizu, and O. Sakai, Phys. Rev. Lett. **76**, 271 (1996).
[4] Y. Tokura and N. Nagaosa, Science **288**, 462 (2000).
[5] F. C. Zhang and T. M. Rice, Phys. Rev. B **37**, 3759(R) (1988).
[6] A. Ramires, P. Coleman, A. H. Nevidomskyy, and A. M. Tsvelik, Phys. Rev. Lett. **109**, 176404 (2012).
[7] S. Nakatsuji *et al.*, Nat. Phys. **4**, 603 (2008).
[8] K. Kuga, Y. Karaki, Y. Matsumoto, Y. Machida, and S. Nakatsuji, Phys. Rev. Lett. **101**, 137004 (2008).
[9] Y. Matsumoto, S. Nakatsuji, K. Kuga, Y. Karaki, N. Horie, Y. Shimura, T. Sakakibara, A. Nevidomskyy, and P. Coleman, Science **331**, 316 (2011).
[10] M. Okawa *et al.*, Phys. Rev. Lett. **104**, 247201 (2010).
[11] T. Tomita, K. Kuga, Y. Uwatoko, P. Coleman, and S. Nakatsuji, Science **349**, 506 (2015).
[12] C. Bareille, S. Suzuki, M. Nakayama, K. Kuroda, A. H. Nevidomskyy, Y. Matsumoto, S. Nakatsuji, T. Kondo, and S. Shin, Phys. Rev. B **97**, 045112 (2018).
[13] A. H. Nevidomskyy and P. Coleman, Phys. Rev. Lett. **102**, 077202 (2009).
[14] A. Sekiyama, Y. Kanai, A. Tanaka, and S. Imada, J. Phys. Soc. Jpn. **88**, 013706 (2019).
[15] T. Mori *et al.*, J. Phys. Soc. Jpn. **83**, 123702 (2014).
[16] Y. Kanai *et al.*, J. Phys. Soc. Jpn. **84**, 073705 (2015).
[17] Y. Matsumoto, K. Kuga, T. Tomita, Y. Karaki, and S. Nakatsuji, Phys. Rev. B **84**, 125126 (2011).
[18] D. A. Shirley, Phys. Rev. B **5**, 4709 (1972).
[19] A. Proctor and P. M. A. Sherwood, Anal. Chem. **54**, 13 (1982).
[20] R. T. Macaluso, S. Nakatsuji, K. Kuga, E. L. Thomas, Y. Machida, Y. Maeno, Z. Fisk, and J. Y. Chan, Chem. Mater. **19**, 1918 (2007).
[21] K. W. H. Stevens, Proc. Phys. Soc. London Sect. A **65**, 209 (1952).
[22] B. T. Thole, G. van der Laan, J. C. Fuggle, G. A. Sawatzky, R. C. Karnatak, and J.-M. Esteva, Phys. Rev. B **32**, 5107 (1985).
[23] A. Tanaka and T. Jo, J. Phys. Soc. Jpn. **63**, 2788 (1994).
[24] R. D. Cowan, *The Theory of Atomic Structure and Spectra* (University of California Press, Berkeley, 1981).
[25] J. Yamaguchi *et al.*, Phys. Rev. B **79**, 125121 (2009).
[26] O. Gunnarsson and K. Schönhammer, Phys. Rev. B **28**, 4315 (1983).
[27] J.-M. Imer and E. Wuilloud, Z. Phys. B **66**, 153 (1987).
[28] M. Yabashi *et al.*, Nucl. Instrum. Methods Phys. Res., Sect. A **467–468**, 678 (2001).
[29] M. Yabashi, K. Tamasaku, and T. Ishikawa, Phys. Rev. Lett. **87**, 140801 (2001).
[30] H. Fujiwara *et al.*, J. Synchrotron Radiat. **23**, 735 (2016).
[31] See Supplemental Material at http://link.aps.org/supplemental/10.1103/PhysRevLett.123.036404 for the sample preparation and the characterization, which also includes Ref. [20], for the evidence of the negligible temperature dependence of LD, which also includes Refs. [15,17], and for the candidates of the extrinsic reason for the suppression of LD, which also includes Refs. [14,23,32–36].
[32] J. Weinen *et al.*, J. Electron Spectrosc. Relat. Phenom. **198**, 6 (2015).
[33] S. M. Goldberg, C. S. Fadley, and S. Kono, J. Electron Spectrosc. Relat. Phenom. **21**, 285 (1981).
[34] S. Hüfner, *Photoelectron Spectroscopy*, 3 ed. (Springer, Berlin, 2003).
[35] M. B. Trzhaskovskaya, V. I. Nefedov, and V. G. Yarzhemsky, At. Data Nucl. Data Tables **77**, 97 (2001).
[36] M. B. Trzhaskovskaya, V. K. Nikulin, V. I. Nefedov, and V. G. Yarzhemsky, At. Data Nucl. Data Tables **92**, 245 (2006).
[37] H. Aratani, Y. Nakatani, H. Fujiwara, M. Kawada, Y. Kanai, K. Yamagami, S. Fujioka, S. Hamamoto, K. Kuga *et al.*, Phys. Rev. B **98**, 121113(R) (2018).
[38] K. Kuga *et al.*, Sci. Adv. **4**, eaao3547 (2018).
[39] K. Deguchi, S. Matsukawa, N. Sato, T. Hattori, K. Ishida, H. Takakura, and T. Ishimasa, Nat. Mater. **11**, 1013 (2012).